Chemical Engineering Journal 155 (2009) 207–214

Contents lists available at ScienceDirect

Chemical Engineering Journal

journal homepage: www.elsevier.com/locate/cej

Hydrodynamic studies on three-phase fluidized bed using CFD analysis

K. Sivaguru, K.M. Meera Sheriffa Begum, N. Anantharaman*

Department of Chemical Engineering, National Institute of Technology, Tiruchirappalli 620015, India

ARTICLE INFO

Article history:
Received 11 March 2007
Received in revised form 24 May 2009
Accepted 17 July 2009

Keywords:
Three-phase fluidization
CFD model
CFD analysis
Porous jump model
Porous zone model

ABSTRACT

Three-phase fluidization refers to fluidization of solid particles by co-current, upward flow of gas and liquid-phases for the purpose of bringing three-phases in contact in a single operation. Due to complications in understanding hydrodynamics of three-phase fluidized bed, CFD analysis is used to predict the hydrodynamics of it. In this study, liquid-phase is water which flows continuously, where as the gas phase is air which is distributed discretely throughout the bed. Ceramic particle of 1 mm diameter, density of 2650 kg/m^3 is used as a solid phase. Excellent mixing, heat and mass transfer rates are the unique features of three-phase fluidized bed. The selection of distributor plays an important role in the quality of fluidization[1]. CFD model is created as the realistic representation of actual fluidized bed. The liquid and solid flow is represented by the mixture model. The air is injected from the bottom of the fluidized by means of discrete phase method (DPM). Simulation results are obtained by using porous jump and porous zone model to represent the distributor. It is found that porous zone model is best applicable in the industries, since stability of operating conditions is achieved even with non-uniform air, water flowrates and with different bed heights(100 mm, 200 mm, 300 mm, 400 mm and 500 mm).

Simulated Pressure drop values of the fluidized bed have good agreement with the experimental findings. As the gas flowrate increases, the pressure drop in the column is decreases, provided the initial bed height, diameter of the column, and liquid flowrate are constant. This is due to decrease in density of the fluid medium in the bed by means of more gas hold up. The approach of the simulated values to the experimental values can be reduced with better understanding the nature of the fluidized bed.

1. Introduction

Three-phase fluidization is a term commonly used for processes where a particulate solid is suspended in an upward co-current flow of gas and liquid. Three-phase fluidization may in some ways be regarded as intermediate to slurry and fixed bed operations in particular with regard to particle size which typically falls within the range from 0.2 mm to 6 mm. The operation is characterized by the advantages and disadvantages common to fluidized bed operations. In general the major advantages are the excellent heat transfer and ease of addition and removal of solids. Solids entrainment and intraphase mixing are potential disadvantages.

In this three-phase study, solid is ceramic particle, liquid-phase is water and gaseous phase is air. In order to understand the hydrodynamics of a fluidized bed operation, it is essential to assess how air flow, liquid flow and solids movement are distributed through out the equipment. The understanding of three-phase flows is still limited due to complicated phenomena underlying interactions between phases such as particle–bubble interactions and the liquid interstitial effect during particle–particle collision. Numerical modeling techniques such as computational fluid dynamics (CFD) provide an important means to obtain this understanding. This study is concerned with the development of a computational model of three-phase flows i.e., in the liquid–solid mixture; the air is injected as bubbles. This simulation work combines the mixture model with discrete bubbles to predict the behavior of the individual phases.

A two-dimensional simulation is developed by using porous zone and porous jump model. Even though the Eularian model is more accurate than the mixture model, porous jump model is not applicable with Eularian model. Hence, for the comparison study between the porous zone and porous jump model, mixture model is chosen for both porous zone and porous jump cases. In this comparison study, it is found that the porous zone model performs better with non-uniform air flowrates. Porous zone modeling is recommended from the industrial scale point of view. From the experiments conducted by varying the air flowrate, it is found that the pressure drop of the bed decreases with increasing air flowrate. This is due to reduction in density of the mixture, as most of the water is replaced by air. Optimum air flowrate selection for better fluidization as well as reducing the power consumption is needed. Simulation results agree with the experimental findings.

* Corresponding author. Tel.: +91 431 2550726; fax: +91 431 2500133.
E-mail address: naramanrect@yahoo.co.in (N. Anantharaman).

1385-8947/$ – see front matter © 2009 Elsevier B.V. All rights reserved.
doi:10.1016/j.cej.2009.07.037

Due to the complex nature of the hydrodynamics of bubbly flow in liquid–solid media, it is difficult to obtain a mechanistic model that can be used to calculate the bubble rise velocity in various physical properties and system parameters [2]. For wide-range predictions of the bubble rising characteristics in liquid–solid suspensions and of the dynamic behavior of gas–liquid–solid fluidization systems including the interactions of individual bubbles and particles, numerical simulations based on the computational fluid dynamics are required.

Numerous numerical simulation works are developed by using CFD codes in the recent years. Such a numerical simulation of gas–liquid–solid fluidization systems using a combined CFD–VOF–DPM method is done by Li et al. [3]. In this study, a new approach is developed to predict the characteristics of the discrete phases. Numerical studies of bubble and particle dynamics in a three-phase fluidized bed at elevated pressures is developed by Zhang et al. [2]. A discrete phase simulation is developed to study the bubble and particle dynamics in the three-phase fluidized bed at high pressures [2]. Li et al. [4] have developed numerical studies of bubble formation dynamics in gas–liquid–solid fluidization at high pressures. Van Sint Annaland et al. [5] have done the work on numerical simulation of gas–liquid–solid flows using a combined front tracking and discrete particle method [5].

2. Computational models

2.1. Liquid-phase equations

The modeling equations for the multiphase flows can be obtained from the Navier–Stokes equations for single-phase flows. Dispersed particles and volume-averaging technique are used to develop a set of partial deferential equations to describe the mass and momentum conservation of individual phases. The volume-averaged forms of the conservation equations can be written as:

Liquid-phase continuity equation:

$$\frac{\partial \varepsilon_\ell}{\partial t} + \nabla(\varepsilon_\ell V) = 0 \tag{1}$$

Liquid-phase momentum equation:

$$\rho_\ell \frac{\partial(\varepsilon_\ell V)}{\partial t} + \rho_\ell \nabla(\varepsilon_\ell VV) = -\nabla P + \nabla(\varepsilon_\ell \tau) + \varepsilon_\ell \rho_\ell g + F_{pf} + F_{bf} \tag{2}$$

where V is the liquid velocity vector, ε_ℓ is the liquid hold up, ρ_ℓ is the liquid density,

P is the scalar pressure, τ is the viscous stress tensor, F_{pf} and F_{bf} are forces acting on the liquid-phase from individual particle and bubble, which can, respectively be obtained using Newton's third law and a continuum surface force (CSF) model.

2.2. Ceramic particle governing equations

2.2.1. Ceramic particle motion equations

The motion of a ceramic particle in the three-phase fluidized bed is given by Lagrangian coordinates. The origin of this coordinate is attached with the center of the moving particle. The particle rotational acceleration or deceleration is negligible during the motion without collision. The force on a particle can be determined exclusively from its interaction with the liquid by choosing reasonable time step. A time step of 10^{-4} s in chosen, which is similar to the concept of Cundall and Strack [6].

The motion of a single particle without collision can be governed by Newton's second law:

$$m_p \frac{dx_p}{dt} = v_p \tag{3}$$

$$m_p \frac{dv_p}{dt} = m_p g - V_p \rho g + F_{fb} + F_{bP} \tag{4}$$

where x_p and v_p are the particle position and velocity, respectively, in Eq. (3) and the four terms on the right-hand side of Eq. (4) are the gravity force, the buoyancy force, the liquid interaction force and the gas–bubble interaction force, respectively.

2.2.2. Total forces on ceramic particle

Total forces acting on the ceramic particle is composed of all applicable forces, including drag, added mass, gravity, buoyancy and Basset history force. The interface force between the particle and gas bubble, F_{bp}, can be obtained by using a bubble-induced force model [2].

The forces acting on a particle from liquid, F_{fp}, include the drag force, the added mass force and the Basset force. The Saffman and Magnus forces are ignored due to small particle size (d_p = 1 mm)

$$F_{fp} = F_D + F_{AM} + F_{BA} \tag{5}$$

It is to be noted that the pressure gradient force is not included in Eq. (5). For consistency (Xu and Yu [7]), this force has been accounted for in the liquid-phase momentum equation given in Eq. (2). The drag force acting on a suspended particle is proportional to the relative velocity between the phases and has the following form

$$F_D = \frac{1}{2} C'_D \rho A \left| V - V_p \right| (V - V_p) \tag{6}$$

where A is the cross-sectional area of the particle to the direction of the incoming flow and C'_D is the effective drag coefficient.

The drag force in the liquid–solid suspension depends strongly on the local liquid hold up in the vicinity of the particle under consideration. The effective drag coefficient can be obtained by the product of the drag coefficient for an isolated particle and a correction factor as given by Wen and Yu [8]:

$$C'_D = C_D \varepsilon_\ell{}^{-4.7} \tag{7}$$

where C_D is a function of the particle Reynolds number (Re_p). For rigid spherical particles the drag coefficient C_D can be estimated by the following equations given by Rowe and Henwood [9]:

$$C_D = 24/Re_p(1 + 0.15Re_p^{0.687}) \quad Re_p < 1000 \tag{8}$$

$$C_D = 0.44 \quad Re_p \geq 1000 \tag{9}$$

The fluid travels along with the particle with same acceleration as that of the particle and exerts additional mass force to the solid mass. For a spherical particle, the volume of the added mass is equal to one-half of the particle volume, V_P.

$$F_{AM} = \frac{1}{2} \rho V_p \frac{d}{dt}(V - V_P) \tag{10}$$

The Basset force induced by the particle acceleration or deceleration in liquid can be expressed as suggested by Mei and Adrian [10]:

$$F_{BA} = 3\pi\mu d_p \int_0^t K(t-\tau) \frac{d(V - V_P)}{dt} d\tau \tag{11}$$

where $K(t-\tau)$ in Eq. (11) is given as

$$K(t-\tau) = \left\{ \left\{ \left[\frac{\pi(t-\tau)\nu}{r_p^2} \right]^{1/4} + \left[\frac{1}{2}\pi \frac{(U + v_p - v)^3}{r_p \nu f_H^3(Re)} (t-\tau)^2 \right]^{1/2} \right\}^{-2} \tag{12}$$

$$f_H(Re) = 0.75 + 0.105Re, \quad Re = Ud_p/\nu \tag{13}$$

where ν the kinematic viscosity of the fluid and U is the mean stream velocity.

2.3. Analysis of ceramic particles collision

When particles move upwards due to fluidization, collision between the particles occurs. In this study, the hard sphere model proposed by Hoomans et al. [11] for gas–solid flow simulation is used for the particle–particle collision is adapted. In this model, collisions between spherical particles are binary and quasi-instantaneous, and there is a sequence of collisions during each time step. This assumption is a very important consideration in the particle–particle collision analysis. The molecular dynamic simulation proposed by Allen and Tidesley [12] is used to locate the minimum flight time of particles before any collision [3].

2.3.1. Effect of liquid shear

The liquid interfacial effect is important when two particles move close to each other in liquid–solid systems than gas–solid systems. This is an important consideration when the distance between two particles is less than $0.1d_p$. Thus, the close-distance interaction model is used to locate the particle contact velocity just before collision, which considers the strong damping effect due to the liquid film before the particles touching each other [3]. The particle normal contact velocity can be described by:

$$\left(1+\frac{1}{2}\frac{\rho}{\rho_p}+\frac{3}{16}\frac{\rho}{\rho_p}\frac{r_p^3}{h^3}\right)\frac{du_p}{dh}=\frac{9\mu f\phi}{2r^2\rho_p}\frac{u_p-u}{u_p}+\frac{9}{32}\frac{\rho}{\rho_p}\frac{r_p^4(u_p-u)\left|u_p-u\right|}{u_p}-\left(1-\frac{\rho}{\rho_p}\right)\frac{g}{u_p}+\frac{9\mu\int_0^t K(t-\tau)\left[d(u_p-u)/dt\right]d\tau}{2r^2\rho_p u_p} \quad (14)$$

where h is the distance between two particles, r_p is the radius of particle, and f (Schiller and Naumann [13]) and Φ are the correction functions and can be expressed as

$$\phi=\exp\left(\left(\frac{Re_p}{1.7}\right)^{0.44}\left(\frac{\rho_p}{\rho}\right)^{0.19}\left(\frac{r_p}{h}\right)^{Re_p^{0.47}}\right) \quad (15)$$

$$f=1+0.15Re_p^{0.687} \quad (16)$$

using the Runge–Kutta method, Eq. (14) can be solved to locate the particle normal contact velocity just before the collision.

2.3.2. Kinetic collision analysis

This kinetic collision analysis is used to obtain velocities of particles after collision. Assuming that the collision occurs between particles a and b, the normal components after collision can be given by the definition of the restitution coefficient and the momentum conservation equation

$$\frac{U_a^{N'}-U_b^{N'}}{U_b^N-U_a^N}=e \quad (17)$$

$$m_aU_a^N+m_bU_a^N=m_aU_a^{N'}+m_bU_b^{N'} \quad (18)$$

where U^N is the normal velocity of the particle (a or b) at the contact point before collision, $U_a^{N'}$ is the normal velocity of the particle (a or b) at the contact point after collision. The value of e can be evaluated from Lattice-Boltzmann simulation [14]. The value of e is not readily obtainable experimentally for the liquid medium compared to that for the gas medium. The simplified Mindlin's contact theory is applied to obtain the tangential components after the collision. If the incident angle, defined as the ratio of the particle–particle relative velocity in the tangential direction to that in the normal direction, is less than the critical angle ($\alpha_{cr}=\tan^{-1}(2f_k)$), where f_k the friction coefficient, the sticking collision occurs

$$U_a^{T'}=U_b^{T'} \quad (19)$$

In other words, the sliding collision occurs, in which (Fan and Zhu, 1998)

$$(U_a^T-U_b^T)-(U_a^{T'}-U_b^{T'})=2f_k(U_a^N-U_b^N) \quad (20)$$

where U^T is the tangential velocity of particle (a or b) at the contact point.

Eqs. (19) or (20) together with the momentum conservation equation, Eq. (21) give rise to the tangential velocities [3]:

$$m_aU_a^T+m_bU_b^T=m_aU_a^{T'}+m_bU_b^{T'} \quad (21)$$

The collision induces the change of particle rotation. The angular velocities after the collision are determined by:

$$\begin{aligned} I_b(\omega_a'-\omega_a)&=m_a(U_a^{T'}-U_a^T)r_a \\ I_b(\omega_b'-\omega_b)&=m_b(U_b^{T'}-U_b^T)r_b \end{aligned} \quad (22)$$

where ω is the angular velocity of the particle (a or b), and I is the moment of inertia defined by $I=2/5(m_pr_p^2)$.

2.4. Interphase couplings

2.4.1. Coupling between gas and liquid-phases

In the three-phase fluidized bed, the interaction between the gas–liquid happens throughout the bed. The gas flows as bubbles in the suspended medium of liquid–solid. Many models explain the coupling of gas–liquid phases. In the gas–liquid free surfaces, the stress boundary condition follows the Laplace equation as:

$$P_s=P-P_v=\sigma K \quad (23)$$

where the surface pressure P_s is the surface tension induced pressure jump across the interface. The continuum surface force model [15] converts the surface force into a volume force within free surfaces. The volume force at the free surfaces is given by the CSF model as:

$$F_{bf}(X,t)=\sigma K(X,t)\nabla F(X,t) \quad (24)$$

So for in the gas–liquid-phases, the volume force is considered to be the interface force in the system.

2.4.2. Coupling between particle and liquid-phases

The interaction between the particle and liquid can be explained by Newton's third law. Based on this law of motion, the total forces acting on particles yield a reaction force on the liquid. Therefore, the momentum transfer from particles to liquid is taken into account by the liquid–particle interaction force term F_{pf} in Eq. (2):

$$F_{pf}=\frac{\sum F_{fb}^k}{\Delta V_{ij}^k}\quad X_P^k\in\Omega_{ij} \quad (25)$$

where subscript ij defines the location of a computational cell, Ω and ΔV are the domain and volume of this cell, respectively. F_{fb} of any individual particle can be expressed by Eq. (5). The liquid properties on the particle are obtained by an area-weighted averaging method based on the properties at the four grid points of the computational cell containing the particle [2].

In the liquid–solid suspension, the liquid hold up ε_ℓ is obtained by subtracting the volume fraction of the particles from that of the liquid–solid suspension in a computational cell. This cell-averaged method is only used to account for ε_ℓ in solving the volume-averaged equations for the liquid-phase i.e., Eqs. (1) and (2). The

particle-centered area averaging method is used to obtain ε_ℓ in solving the particle phase equation i.e., Eq. (7). A correlation based on the comparison between a hexagonal lattice and an FCC unit cube [11] is used to modify ε_ℓ from two-dimensional to three-dimensional approach. From this, it is possible that to predict the characteristics in three-dimensional simulations [2].

2.4.3. Coupling between particle and gas phases

Due to discrete bubbly phase of the gas, the interaction is not significant as with liquid–solid interactions. The surface tension force also plays an important role on the particles through the liquid film when particles move close to the gas–liquid interface. The size of computational cell is larger than the thickness of the film of gas–liquid interface, so that bubble-induced force model (BIF) is applied to the particle:

$$F_{bp} = V_p \sigma K(X, t) \nabla F(X, t) \quad (26)$$

This BIF should be more in order to avoid bubble breakage. If the particle overcomes this bubble-induced force, the particle would penetrate the bubble surface. The penetrating particle breaks the bubble surface momentarily upon contact. If the penetrating particle is small, the bubble may recover its original shape upon particle penetration [16]. However, if penetrating particle is large, the bubble breakage may take place [5].

3. Experimental setup

3.1. Fluidized bed column

A schematic diagram of the experimental set-up is shown in Fig. 1. The fluidized bed column is 1000 mm length and 25.4 mm in diameter. The liquid flowrate was measured with pre calibrated rotameter and the gas was fed to the column through a pressure regulator and a calibrated rotameter. The gas and the liquid streams merged and passed through an expansion cone. The mixing section and the grid ensured that gas and liquid were well mixed and evenly distributed into the bed. A three-phase separator at the top of the column, allowed experiments to be carried out for a very wide range of operating conditions and allow the gas to escape and liquid to be recirculated.

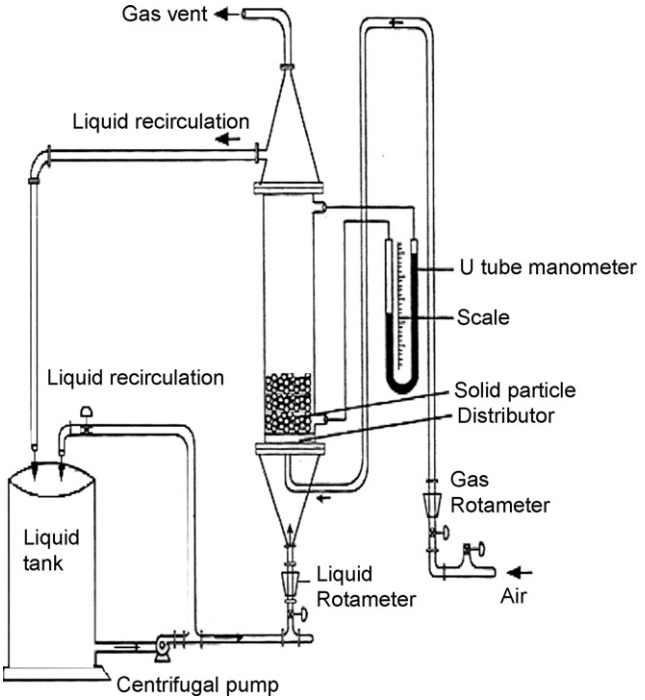

Fig. 1. Experimental setup.

3.1.1. Pressure measurement

The pressure drop across the bed was measured with the help of a U-tube manometer.

3.1.2. Bed height

Experiments were carried out at different bed heights of 100 mm to 500 mm with the interval of 100 mm and the pressure drop studies were carried out on the three-phase fluidized bed, by varying the liquid and gas flowrates and the bed behavior was observed.

3.2. Distributor plate

3.2.1. Functions of the distributor

Distributor plate is one of the most critical design factors. Many studies report on the critical role of the distributor in fluidized bed systems. A substantial proportion of the difficulties encountered in fluidized bed processes can be attributed to inadequate distributor design or malfunctions in operation.

3.2.2. Pressure drop across the distributor

The design of a distributor in terms of required pressure drop is directly or indirectly influenced by a more number of variables such as pressure drop across the particle bed, bed weight, bed height, bed expansion ratio, fluidizing gas flowrate, bed material particle type, particle size and distribution, particle density, distributor geometry and thickness.

In order to achieve a homogeneous fluidizing gas flow over the entire cross-section of the bed, the pressure drop across the distributor should be large enough to guarantee that the gas flowrate through the distributor is relatively undisturbed by the bed pressure fluctuations above the grid or the inherent resistance of rearrangement for gas below the grid [1]. The power consumption and the cost for the compressor also increase with higher distributor pressure drop. The selection of a suitable distributor is important through an optimization procedure.

4. CFD model of the fluidized bed

4.1. Computational grid generation

Prior to the CFD calculations, the geometry was defined and a grid was generated using Gambit 2.1.4, the pre-processor and mesh generator for the CFD solver. CFD model of the fluidized bed domain is a realistic representation of the lab-scale fluidized bed. The modeling includes air inlet, distributor, cylindrical extension and air outlet can be distinguished sequentially.

At these locations, the largest gradients were expected to occur, so mesh refinement was applied, boundary layers in the vicinity of the distributor and an increased number of nodes near the walls. The mesh quality was evaluated using the Equiangular Skew (QEAS) criterion, which is a normalized measure of the element skewness. Otherwise it may be undesirable as it may impede solution convergence and accuracy. For all generated 3-D meshes, the QEAS of at least 90% of the control volumes was lower than or equal to 0.4. Therefore, the overall mesh quality could be considered very well. The complete domain was conceived as a fluid zone. After meshing the domain, the grid was imported into Fluent 6.1.20 (Fluent), the CFD solver used in this study.

4.1.1. CFD simulation with the porous jump boundary condition

In porous jump boundary condition, mixture model in multiphase simulation is chosen, since porous jump is not applicable

with Eulerian model. The mixture model is a simplified multiphase model that can be used to model multiphase flows. In the multiphase flow, phases move at different velocities, but assume local equilibrium over short spatial length scales. The coupling between the phases should be strong. It can also be used to model homogeneous multiphase flows with very strong coupling and the phases moving at the same velocity.

4.1.2. CFD simulation with the porous zone boundary condition

In porous zone boundary condition mixture model is chosen for the CFD simulations. While comparing the porous zone and porous jump model, all the parameters are to be kept similar. As we have seen already, the porous jump model is not applicable for the Eulerian model. The mixture multiphase model in Fluent allows for the modeling of multiple separate, yet interacting phases. The phases can be liquids, gases, or solids in nearly any combination. A mixture treatment is used for each phase, in contrast to the Lagrangian treatment that is used for the discrete phase model. With the mixture multiphase model, the number of secondary phases is limited only by memory requirements and convergence behavior. Any number of secondary phases can be modeled, provided that sufficient memory is available.

4.2. CFD solver

CFD simulations were performed using a single-precision, unsteady-state, segregated, implicit solver. To reduce numerical diffusion, a second-order upwind scheme was selected for the discretisation of the momentum equations. The relationship between velocity and pressure correction was calculated using the standard algorithm. Default values for all under-relaxation factors were applied. Convergence was evaluated in two ways: (1) by following the scaled residuals of each conserved variable and (2) by observing the evolution in facet average static pressure in a face upstream and downstream of the distributor. A solution was considered converged (1) when the scaled residuals had dropped six orders of magnitude for the energy equation and three orders of magnitude for all other simulated variables and (2) when the facet average static pressure in both faces had levelled off.

5. Result and discussions

5.1. CFD simulation results

5.1.1. Influence of boundary condition specification

The CFD results presented below were obtained with the two-dimensional computational domain. These results were obtained with a boundary condition of velocity for water at the inlet. The volume fraction of the solid at the initial, were found to be 0.6 in the actual fluidized bed and is given as input. The velocity at the inlet for water and air as measured with rotameter in the actual studies were used. These values are given as input to the Fluent to find out the pressure drop in the fluidized bed. The experimental and simulated values of the pressure drop are compared and results presented.

5.2. CFD simulation results with the porous jump boundary condition

The thickness and the permeability and the pressure-jump coefficient of the distributor were entered as inputs for the porous jump boundary condition. The important consideration to be taken in this simulation is that porous jump model is applicable to the face and not for cell zone. Fluent 2-D simulations were carried out for a different bed height 100 mm to 500 mm with the interval of 100 mm. The pressure outlet boundary condition was set at 0 pa gauge pressure for this simulation i.e., the fluid which is coming out of the fluidized bed is at atmospheric pressure. Careful selection of the air flowrate will help to prevent particles in the fluidized bed from becoming elutriated or entrapped in the filter housing.

The observed effect is a non-uniform air flow which is redirected into the opposite direction on crossing the air distributor. This condition was not considered to be realistic. Although the pressure drop as a function of the air flowrate was found to be relatively in good agreement with experimental measurements, it was observed that the use of a porous jump boundary condition to model the distributor behavior was not appropriate in this experimental configuration.

5.3. CFD simulation results with the porous zone boundary condition

CFD simulations were performed for a 7 mm porous zone thickness, taking into account the physical thickness of the distributors and combining the values for the impermeability and the inertial resistance. The distributor characteristics for the distributors modeled as a porous zone are

Porous zone thickness is 0.007 m,

$$Dz = 7.54e + 08\ \mathrm{m}^{-2},\ Cz = 2361\ \mathrm{m}^{-1}.$$

The boundary conditions are similar to the porous jump model except the porosity of the fluid in the porous zone model. The distribution of the air–water is more uniform than porous jump model, but more pressure drop in the distributor is observed. Due to higher pressure drop, the power consumption i.e., to pump water and air into the fluidized bed is more. Optimization of cost involved between the uniform fluidization and power spent is necessary. In this porous zone model, it is observed that CFD modeling of the air–water distributor resulted in a physically possible pattern even for an unequal contacting in the distributor. The use of smaller values of zone thickness resulted in a somewhat high mesh density across the distributor and no difference in the simulated air flow pattern was found. Convergence is delayed due to lower value of porous zone thickness and hence an optimized value of thickness has to be given as input.

5.4. Comparative studies on porous zone and porous jump models

Simulation works were done by varying the bed height. The bed height varied from 100 mm to 500 mm with the interval of 100 mm. The plots shown below are obtained at the middle of the bed by means of surface creation.

5.4.1. Radial distance vs. dynamic pressure

In the plot of radial distance vs. dynamic pressure as shown in Figs. 2 and 3, as the bed height increases the dynamic pressure increases in both porous and porous jump cases. The dynamic pressure of the porous jump model is more than the porous model. From this it is concluded that the pressure drop is more in the case of the porous zone model. The main purpose of the distributor is to ensure uniform flow pattern in the fluidized bed. This requires more pressure drop across the distributor. From the pressure drop point of view, the best model is porous zone model. But at the same time, it is very important that the power consumption should be low.

5.4.2. Radial distance vs. velocity of the mixture

The plot shown in Figs. 4 and 5 is radial distance vs. velocity of the mixture. As the bed height increases the velocity of the mixture also increases due to reduction of the gas–liquid hold up in the bed. The gas and liquid move freely on the surfaces of the ceramic solid particle. The velocity of the mixture is less for porous zone

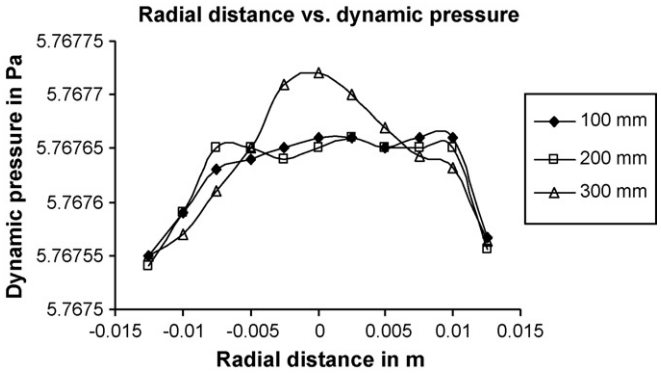

Fig. 2. Variation of dynamic pressure with radial distance – porous zone model.

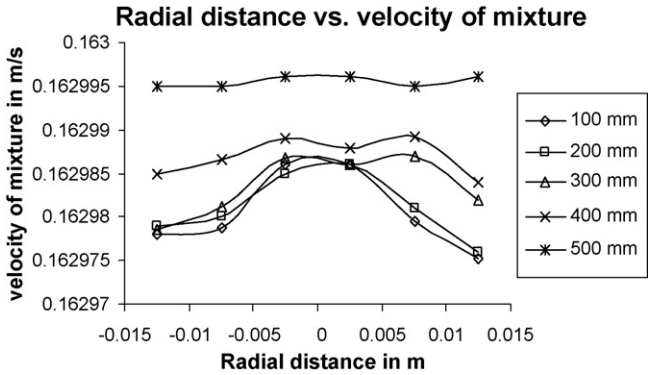

Fig. 5. Variation of velocity of the mixture with radial distance – porous jump model.

model due more pressure drop, but the variation in the velocity of the mixture is less in this case. In the case of porous jump model, the velocity of the mixture profile shape matches with the actual case but the variation is more when compared to the porous jump model. From this, it is known that for uniform air–water flowrates the porous jump model is better than porous zone model. Obviously from the industrial scale point of view, air–water variation is more. So from the industrial point of view the porous zone is better than porous jump model.

5.4.3. Radial distance vs. velocity of water

The plot shown in Figs. 6 and 7 is radial distance vs. velocity of water. In this case also as the bed height increases the velocity of the water also increases. The velocity of water varies more in the case of porous jump model when compared to the porous zone model. The velocity profile in the porous jump model obeys with the actual case, but here also it is observed that the variation is more. When the fluctuation is more, the type of distributor of porous jump model is not the correct option.

5.4.4. Radial distance vs. velocity of solids

Figs. 8 and 9 show the plot of radial distance vs. velocity of solids. As the bed height increases the velocity of the solids in the down ward direction also increases, because of increased velocity of gas–liquid-phases with the bed height. Initially solids do not posses any velocity. After some period of time, the solids posses some velocity which is obtained from the gas–liquid-phases (frictional velocity). In this case also for porous jump model, the velocity of solids varies more with bed height when compared to the porous zone model. The velocity profile in the porous jump model obeys with the actual case, but here also it is observed that the variation is more. When the fluctuation is more, porous jump model is not the required distributor type.

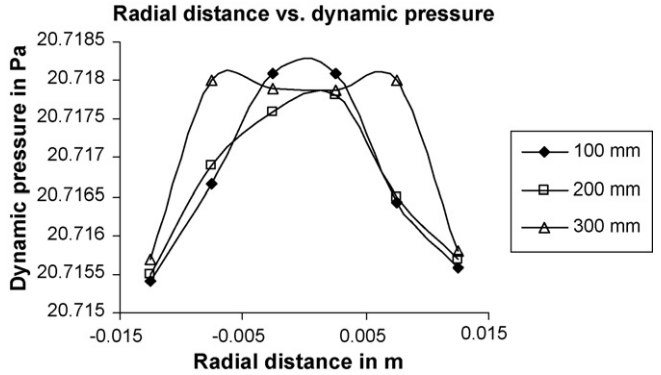

Fig. 3. Variation of dynamic pressure with radial distance – porous jump model.

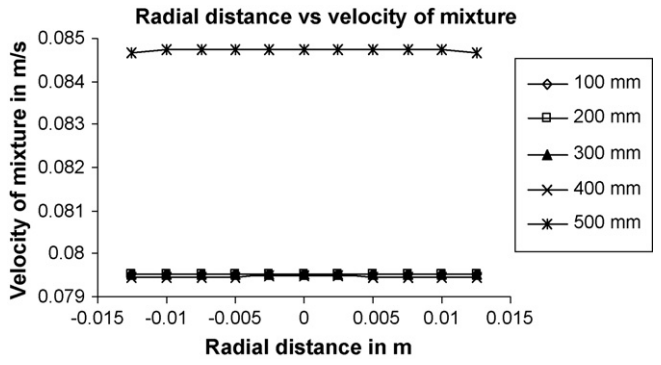

Fig. 4. Variation of velocity of the mixture with radial distance – porous zone model.

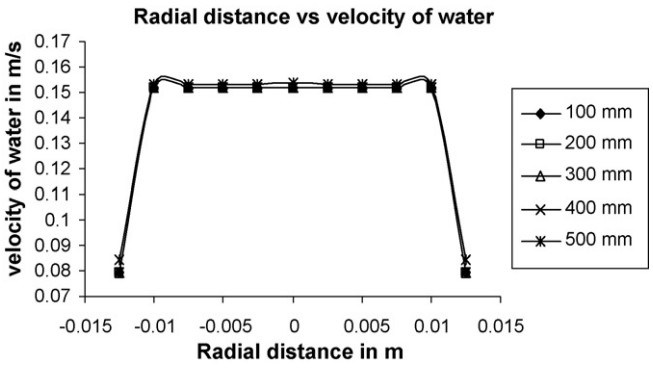

Fig. 6. Variation of velocity of water with radial distance – porous zone model.

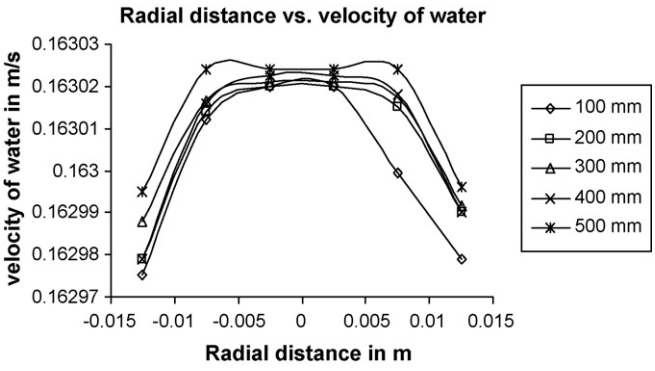

Fig. 7. Variation of velocity of water with radial distance – porous jump model.

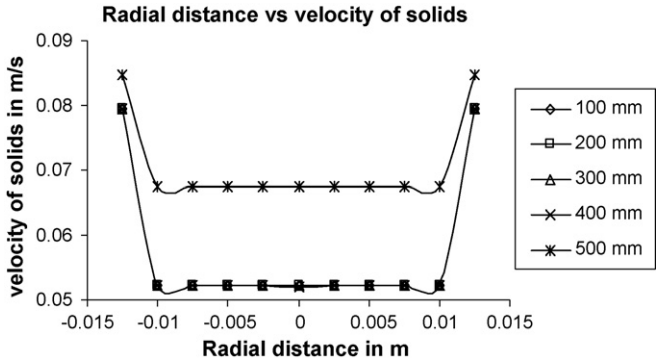

Fig. 8. Variation of velocity of solids with radial distance – porous zone model.

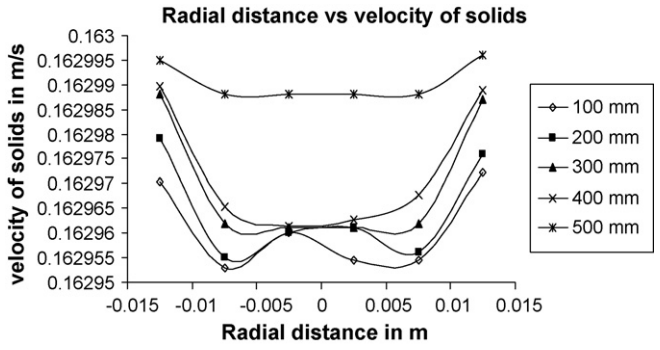

Fig. 9. Variation of velocity of solids with radial distance – porous jump model.

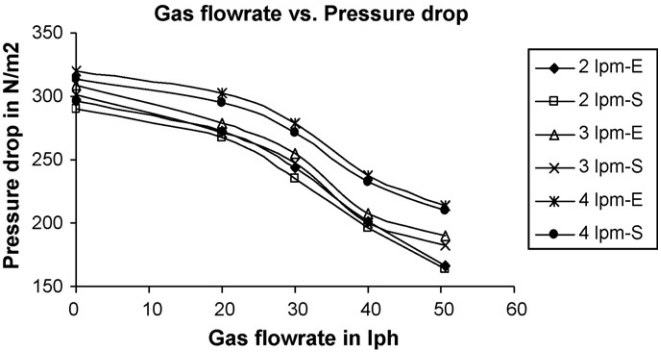

Fig. 10. Variation of pressure drop (N/m^2) with gas flowrate (lpm) (bed height: 100 mm, E: experimental, S: simulated).

As the bed height of solids increases, the solid fraction in the middle of the bed increases due to fluidization of solids. As the gas flowrate increases the solid fraction increases till a particular stage, afterwards the entrainment starts.

5.5. Experimental and simulated values

5.5.1. Gas flowrate vs. pressure drop

The pressure drops are measured at various heights i.e., above the gas distributor and the other near the top of the fluidizing column as a function of superficial gas velocity with the secondary fluid flow as constant. Both the experimental and simulated pressure drops are shown in Figs. 10–14 for bed heights varying from 100 mm to 500 mm. Then the pressure drop in the lower region decreases with the increase in the gas flowrate, where as in the upper region of the riser the pressure drop almost remains constant to some extent and increases suddenly indicating that particles have been entrained to that section due to dense phase expansion.

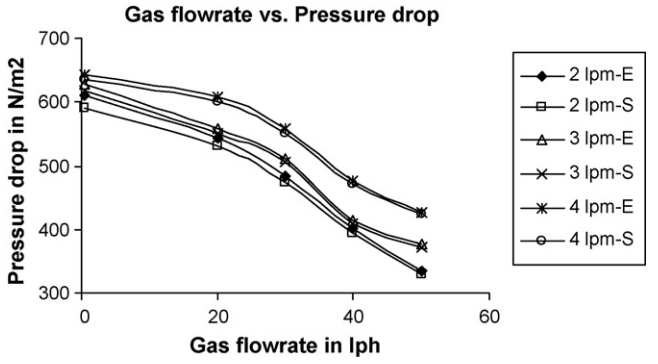

Fig. 11. Variation of pressure drop (N/m^2) with gas flowrate (lpm) (bed height: 200 mm, E: experimental, S: simulated).

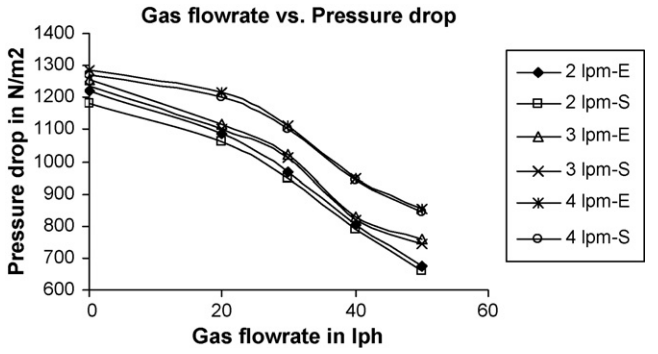

Fig. 12. Variation of pressure drop (N/m^2) with gas flowrate (lpm) (bed height: 300 mm, E: experimental, S: simulated).

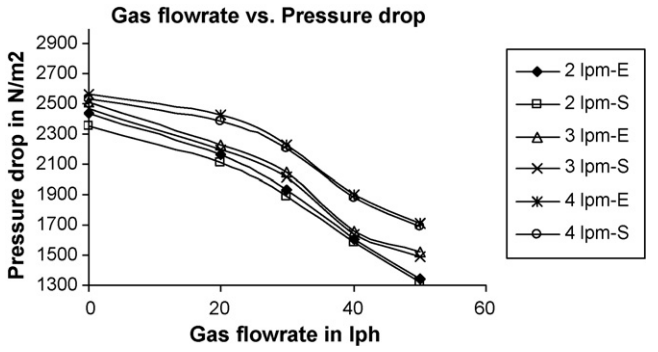

Fig. 13. Variation of pressure drop (N/m^2) with gas flowrate (lpm) (bed height: 400 mm, E: experimental, S: simulated).

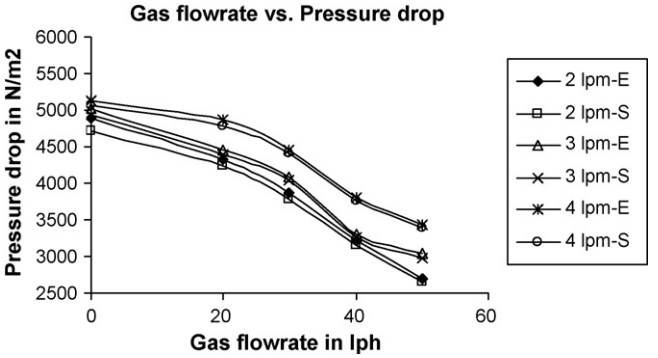

Fig. 14. Variation of pressure drop (N/m^2) with gas flowrate (lpm) (bed height: 500 mm, E: experimental, S: simulated).

Solids are carried over when superficial velocity approaches the terminal velocity. Beyond this point the solids will be completely entrained leaving the total bed vacant. Therefore velocity of single particle can be safely taken as the lowest limit of the superficial liquid velocity required for the three-phase fluidized bed.

With further increase in the superficial velocity the pressure gradient at the upper section starts to drop off due to the uniform distribution of solids over the bed and at a particular flowrate the pressure drop will be zero. This is obtained when the bed is in complete fluidized state.

5.5.2. Effect of superficial flowrates on pressure drop

The pressure drop of the column is decrease for an increase in air flowrate at a constant liquid flowrate. Initially the bed is fluidized by liquid and at this stage the bed remains the normal fluidized bed. As the gas is supplied in, the bubble formation takes place. At low velocities the bubble size is small. As bubble rises it carries both solid particles and liquid droplets with it. Due to more gas hold up in the column, the density of the fluid medium decreases, hence t he pressure drop decreases. Experiments are conducted by varying the bed height and compared with the simulated values. It is found that as bed height increases, pressure drop in the bed increases and Simulated values of pressure drop are less than the experimental values due to all frictional resistance which is present in actual case and cannot be evaluated by simulation results.

6. Conclusion

For uniform air–water flowrate, porous jump model is better than porous zone model. Obviously from industrial point of view porous zone is better than porous jump model, due to more variation of air–water flowrate in industries. As the gas flowrate increases with constant liquid flowrate, the pressure drop of the column decreases. This is due to reduced density in the bed since more gas hold up is in the bed. Simulated values of pressure drop are less than the experimental values due to all frictional resistance which is present in actual and cannot be evaluated by simulation results.

References

[1] F. Depypere, J.G. Pieters, K. Dewettinck, CFD analysis of air distribution in fluidized bed equipment, Powder Technology 145 (2004) 176–189.
[2] J. Zhang, Y. Li, L.-S. Fan, Numerical studies of bubble and particle dynamics in a three-phase fluidized bed at elevated pressures, Powder Technology 112 (2000) 46–56.
[3] Y. Li, J. Zhang, L.-S. Fan, Numerical simulation of gas–liquid–solid fluidization systems using a combined CFD–VOF–DPM method: bubble wake behaviour, Chemical Engineering Science 54 (1999) 5101–5107.
[4] Y. Li, G.Q. Yang, J.P. Zhang, L.-S. Fan, Numerical studies of bubble formation dynamics in gas–liquid–solid fluidization at high pressures, Powder Technology 116 (2001) 246–260.
[5] M. Van Sint Annaland, N.G. Deen, J.A.M. Kuipers, Numerical simulation of gas–liquid–solid flows using a combined front tracking and discrete particle method, Chemical Engineering Science 60 (2005) 6188–6198.
[6] P.A. Cundall, O.D.L. Strack, A discrete numerical model for granular assemblies, Geotechnique 29 (1979) 47–65.
[7] B.H. Xu, A.B. Yu, Numerical study of the forces acting on individual particles in gas fluidized beds, Fluidization-IX (1998) 461–468.
[8] C.Y. Wen, Y.H. Yu, A generalized method for predicting the minimum fluidization velocity, AICHE J. 12 (3) (1996) 610–612.
[9] P.N. Rowe, G.A. Henwood, Drag forces in a hydraulic model of a fluidized bed Part-I, Trans. Inst. Chem. Eng. 39 (1961) 43–54.
[10] R. Mei, R.J. Adrian, Flow past a sphere with an oscillation in the free-stream velocity and unsteady drag at finite Reynolds number, Journal of Fluid Mechanics 237 (1992) 323–341.
[11] B.P.B. Hoomans, J.A.M. Kuipers, W.J. Briels, W.P.M. van Swaaij, Discrete particle simulation of bubble and slug formation in a two-dimensional gas-fluidized bed: A hard-sphere approach, Journal of Chemical Engineering Science 51 (1996) 99–118.
[12] M.P. Allen, D.J. Tildesley, Computer Simulation of Liquids, Oxford Science Publications, 1987.
[13] L. Schiller, Z. Naumann, A Drag Coefficient Correlation, Z. Ver. Deutsch. Ing. 77 (1933) 318–320.
[14] S. Chen, G. Doolen, Lattice Boltzmann method for fluid flows, Annual Review of Fluid Mechanics 30 (1998) 329–364.
[15] J.U. Brackbill, D. Kothe, C. Zemach, A continuum method for modeling surface tension, Journal of computational physics 100 (1992) 335–354.
[16] Y.M. Chen, L.S. Fan, Bubble breakage due to particle collision in a liquid medium particle wettability effects, Chemical Engineering Science 44 (1989) 2762–2767.